AL47 - Modelling Study of Bath Agitation by Bubbles and its Effect on Bath-Metal Interface Stability

Samuel Théberge[1], Lukas Dion[2], László Kiss[3], Thomas Roger[4], Simon-Olivier Tremblay[5], Sébastien Guérard[6] and Jean-François Bilodeau[7]

1. Master student
University Research Centre on Aluminum (CURAL) – Aluminum Research Centre (REGAL) - Université du Québec à Chicoutimi (UQAC), Chicoutimi, Canada
2. Professor
3. Professor emeritus
4. Post-doctorat
5. Research professional
Université du Québec à Chicoutimi (UQAC), Chicoutimi, Canada
6. Research scientist
7. Research scientist
Arvida Research and Development Center, Arvida, Canada
Corresponding author: stheberge2@etu.uqac.ca

Abstract

Two dimensional simulations of the carbon dioxide production and its bubble flow under an aluminum electrolysis anode were performed using a CFD model on ANSYS FLUENT. This model calculates the local current density to determine the local gas production rate. Building on previous research from the group, the bubble behavior underneath the anodes is replicated along with their escape from electrolytic bath towards the central and side channels.

The simulations investigate the system's response to the bubble behavior as a function of the turbulence it generates and its effect on the bath-metal interface stability. The results are consistent with previous publications regarding the frequency of bubble generation and evacuation along with the corresponding response on the voltage variations under the anode as a function of time. Further analysis has allowed a better understanding of the mixing in the center channel and the side channels as well as a perturbation indicator for the bath-metal interface (BMI) caused by the bubbles escaping from under the anode.

Finally, a sensitivity analysis of different key parameters such as anode geometry, anode-cathode distance, and central channel size, was performed to pinpoint the conditions in favor of an increased mixing index (better alumina dissolution), while also highlighting the conditions that minimize the BMI perturbation (increased current efficiency). A discussion on the effect of these parameters and recommendations leading to potential improvements for the Hall-Héroult process are presented.

Keywords: Computational fluid dynamics, Aluminum reduction cell, CO_2 production, Bubble flow.

1. Introduction

1.1 Generality

The Hall-Héroult process is a process invented simultaneously by Charles Hall and Paul Héroult in 1886. With this process, aluminum is produced by electrolyzing alumina (Al_2O_3). A cryolite mixture is used to dissolve the alumina and allow the electrolysis reactions at a much lower

temperature (950-970 °C) then its melting temperature (2072 °C) [1, 2]. Aluminum is produced in industrial cells where the main components are illustrated in Figure 1.

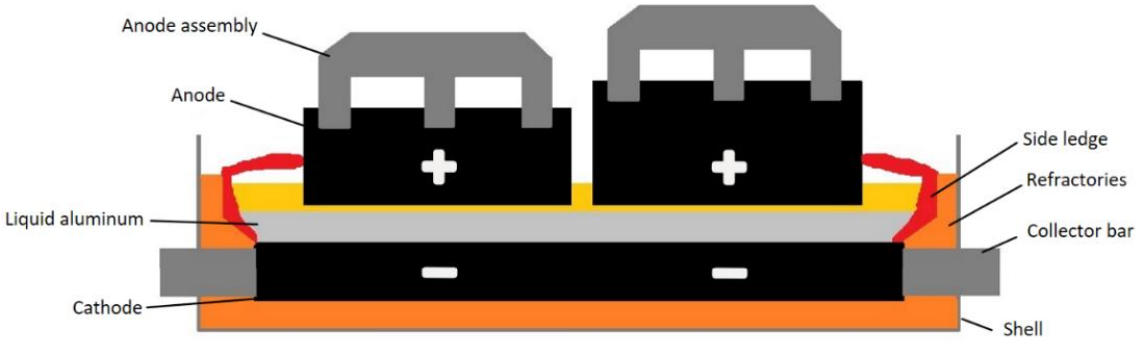

Figure 1. Electrolysis cell main components.

In the electrolytic cell, a current circulates from the anode to the cathode, producing the following generalized reduction reaction in the cell:

$$2Al_2O_3 + 3C = 4Al + 3CO_2 \quad (1)$$

While the reactions occurring are much more complex, the main products of this reaction are aluminum and carbon dioxide (CO_2) gas. The aluminum produced joins the liquid aluminum already present at the bottom of the cell due to gravity forces. On the other hand, CO_2 is formed on the lower surface of the anode and tends to rise to the surface.

1.2 Gas Production and Bubble Flow

During aluminum electrolysis using the Hall-Héroult process, various gases are produced in addition to CO_2. The resulting gas flow has the advantage of stirring the electrolytic bath, particularly in the cell's central channel, which promotes alumina dissolution and distribution [3]. However, they also produce significant disadvantages, such as voltage fluctuation due to electrical insulation between anode and cathode [4-7], along with a significant greenhouse gas contribution [1, 2]. It is therefore important to understand the behavior of bubbles to promote optimal mixing conditions while avoiding excessive electrical insulation.

Among the gases found in an electrolytic cell, the most commons are CO_2, CO, HF, SO_2, CF_4 and C_2F_6. The most concentrated gas generated is CO_2, directly proportional to the mass of metal produced as shown in equation 1. This reaction is the only one considered for the initial step of the work presented in this paper. On the other hand, a better understanding of the flow of CO_2 bubbles may help to improve the dissolution of alumina in the smelting cell and thus reducing the generation of perfluorocarbons.

The layer of bubbles is around 5 mm thick [5, 8-10]. While bubble nucleation occurs at various sites under the anode. Initially small in size, they grow as gas is generated, and coalescence between the bubbles takes place, leading to even larger bubbles. At some point, they escape from the bottom surface of the anode, leading to continuous variations in potential (between 0.05 and 0.2 V) [4].

To facilitate the bubble removal, anode slots are usually cut into the bottom of the anodes for a significant part of their life. However, since the model presented in this work is two-dimensional, the effect of the slots has not been represented, discussion on the impact of this hypothesis is presented further in the analysis.

1.3 Current Efficiency

In industrial cells, the theoretical amount of aluminum produced under a specific cell current is calculated according to Faraday's law. Therefore, smelters try to achieve an efficiency close to that theoretical maximum to enhance the mass of metal produced for the same amount of energy, thus reducing overall cost. In modern cells, typical current efficiencies reported are between 90 % and 95 % [1].

There are numerous causes that may reduce the overall current efficiency of a cell, but a significant one to consider is the reverse-reaction that may occur in the smelting cell. Specifically, the aluminum produced can dissolve in the electrolyte to a certain extent (up to 0.1 % by mass) [1, 4]. This aluminum is present in the form of fine droplets (metal fog) which can get in contact with CO_2 bubbles produced under the anode. Then, a reverse reaction to the original electrolysis takes place, transforming the aluminum back into alumina:

$$2Al + 3CO_2 = Al_2O_3 + 3CO \quad (2)$$

Current efficiency has been widely studied in the field, and some input parameters were highlighted as contributors with a significant role on the resulting current efficiency. For example, this reaction will take place to a greater extent especially if the bath temperature is higher, which increases the rate of aluminum dissolution in the electrolyte. The reaction will also be greater if the metal is closer (low anode-cathode distance (ACD)) to the bottom surface of the anode, and thus to the CO_2 bubbles. Indeed, if the metal touches the CO_2 below the anode, a large amount of aluminum will be reoxidized to alumina. This is why it is so important to understand the movements of the bath-metal interface (BMI), in order to minimize these unintended contacts.

2. Literature Review

Numerous authors have presented numerical models for simulating the flow or current distribution under carbon anodes. All these authors have produced their models in a precise manner with specifically targeted observations.

Einarsrud et al. [11] produced a 3D model of an entire cell using ANSYS FLUENT. Their model simulates fluid flow, current distribution, magnetohydrodynamics (MHD) and alumina distribution in the transient domain. The aims of this study are to analyze the transition time to the steady state MHD and its deformation, to know the bubble escape frequency and gas accumulation under the anode as a function of anode inclination and current density, to calculate the velocity of the fluids and to calculate the alumina concentration at each location in the cell as a function of time.

Zhang et al. [9, 12] produced two similar models (2013 and 2014) in which they simulated a half-anode in 2D with ANSYS FLUENT. The 2013 study focuses on the effect of the bubble size on the bubble flow. This model is therefore a transient fluid model in which a single bubble is represented. The 2014 study focuses on the electrical side of the process. In this model, bubbles are placed under the anode, and the current is analyzed in steady state. The aim of this study is to investigate the effect of the anode bubble coverage, bubble size and bubble thickness on current distribution and voltage drop.

Zhan et al. [13] produced two 3D models. One model features an entire smelting cell, while the other contains just three anodes. This study focuses on fluid flow in the transient domain. The main aim is to reproduce and visualize bubble flows in the electrolytic cell and to output the velocity vector fields.

Feng et al. [14] have produced a 3D model of three anodes. The aim is to visualize the transient bubble flow. The ANSYS CFX module was preferred to FLUENT. Also, in this study, bubble flow was visualized with PIV measurements in an analogous water-air model. The authors studied the effect of slots on bubble flow.

Severo et al. [10] modeled a single anode and an entire cell in 3D using ANSYS CFX. The model simulates the production of bubbles under the anode and their transient flow. The author used a steady-state MHD velocity determined in one of their previous models to represent the effect of the metal movement on the bath with a moving wall condition at the cathode. The main aim of this study is to analyze the effect of slots on bubble flow.

Cubeddu et al. [15] used OpenFoam to model two anodes in 2D. Their model simulates bubble production as a function of bubble coverage under the anode, and the flow of the bubbles produced. The main result analyzed by the authors is the current distribution under the anodes.

Table 1 presents a summary of the turbulence models used by the authors, as well as if they modeled the bath-metal interface.

Table 1. Summary of the turbulence models used by the authors [9-15].

Author	Turbulence model	Presence of a bath-metal interface
Einarsrud et al.	k-ε	Yes
Zhang et al. (2013)	Not applicable	No
Zhang et al. (2014)	Not applicable	Yes
Zhan et al.	k-ε	No
Feng et al.	k-ε	No
Severo et al.	k-ε	No
Cubeddu et al.	Not determined	Yes

According to previous research, the k-ε model is widely used for this type of simulation. This choice is logical since this model is perfectly suited for resolving moderately turbulent flows, such as the bubble flow in an electrolysis cell that has a low velocity [16].

Table 1 also shows that some authors have modeled the bath-metal interface. However, few studied the effect of bubble escape on its deformation. Thus, this work attempts to fill this information which can lead to optimization opportunities to reduce instability in the cells and increase current efficiency.

Similarly, Table 2 presents a summary of the important boundary conditions of the model.

Table 2. Summary of the boundary conditions [9-15].

	Fluidic boundary conditions	Electrical boundary conditions	
Authors	**Under the anode**	**Anode**	**Cathode**
Einarsrud et al.	User-defined function (UDF)	0V	Imposed current density
Zhang et al. (2013)	Mass inlet	Not applicable	Not applicable
Zhang et al. (2014)	Not applicable	Imposed current density	0V (at collector bar)
Zhan et al.	Mass inlet	Not applicable	Not applicable
Feng et al.	Mass inlet	Not applicable	Not applicable
Severo et al.	Mass inlet	Not applicable	Not applicable
Cubeddu et al.	Mass inlet	Imposed potential	Imposed electric potential gradient

Regarding the electrical boundary conditions, the authors utilize three different methods: impose a voltage difference between the electrodes, impose a current at the anode or impose a current at the cathode. These three methods have their advantages and inconveniences when it comes to representing the reality. Furthermore, the fluidic boundary conditions beneath the anode (which corresponds to bubble production) generally involve inlet mass flow.

3. Modelling Method

3.1 Modelling Parameters Used

The ANSYS FLUENT commercial software is used for this model. The aim is to simulate the current distribution under an aluminum electrolysis anode, in order to proportionally generate CO_2 bubbles as a function of the calculated current and to simulate bubble flow under the anode in the side and center channels. The Volume of Fluid method combined with Level Set was chosen for this purpose. The Volume of Fluid (VOF) method is widely used to simulate flows between immiscible fluids [10, 11, 17].

The standard k-ε turbulence model has been retained based on the ANSYS FLUENT user manual's information in agreement with similar research from several other authors. In addition, three fluids are represented in this model: carbon dioxide (gas), electrolytic bath (liquid), and aluminum (liquid). The aim of representing these three fluids is firstly to see the flow of bubbles, and secondly to observe the agitation at the BMI resulting from the bubble flow perturbations.

To simulate a bubble production representative of realistic cell conditions, the electrical module is activated to determine the current flow between the anode and cathode. The aim is to determine local bubble production based on current flow. The developed model considers a two-dimensional slice of the cell in the width direction as shown in Figure 2. A two-dimensional geometry was chosen initially to gain knowledge and initial understanding of the influence of different factors on the results of interest. This knowledge will be used to produce a 3D model that properly represents the industrial conditions.

Finally, a total of 20 seconds has been simulated for each case studied. Element sizes are 2 mm, and the imposed time step is 0.001 s. The elapsed time was sufficient to reach a steady-state flow long enough to generate the data needed for the analysis. The time required to reach steady state was determined by observing the anode bubble coverage, which stabilizes after a certain time.

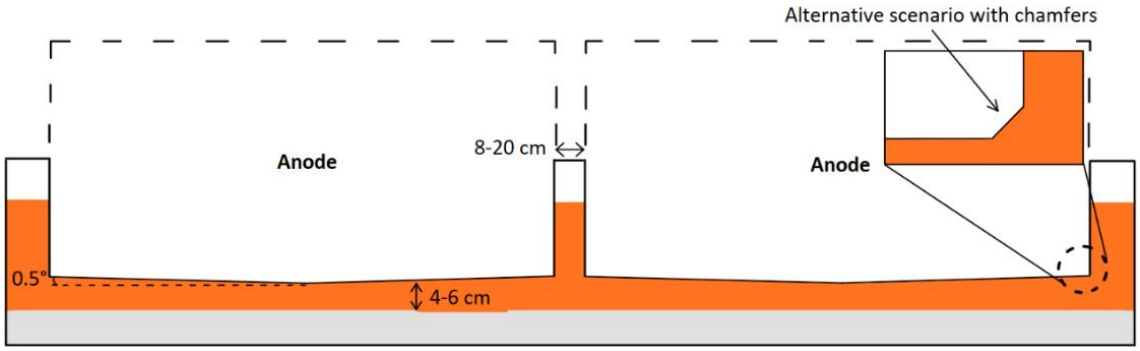

Figure 2. Illustration of the model considered (components not up to scale).

One particularity of this preliminary study is that the metal height is much lower than the bath height. Although the metal level is generally on par with the bath level, using this depth considerably reduces calculation times while still allows to observe the desired effect which is the ripple effect on the upper surface of the liquid aluminum. The width of the central channel is a

variable parameter in this study, ranging from 8 to 20 cm. Similarly, the mean ACD is a variable parameter, between 4 cm and 6 cm. An angle of 0.5° is used to model the bottom surface of the anode, representing erosion caused by the process of electrolysis.

3.2 Boundary Conditions

To make this model, electrical and flow boundary conditions had to be set. Figure 3 gives a visual presentation of these boundary conditions.

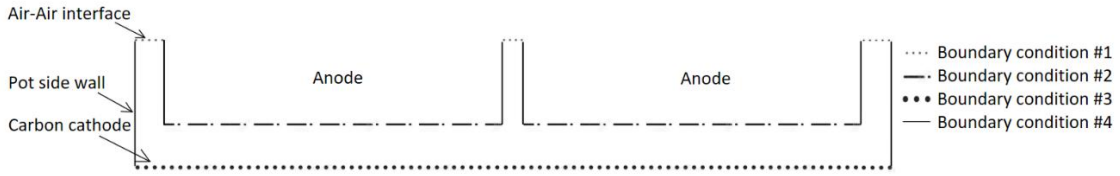

Figure 3. Boundary conditions.

Four different boundary conditions exist. The three surfaces at the top of the figure are where the gas is exchanged with the surrounding environment. The two surfaces under the anodes correspond to a zone where the current circulates and the gas is generated. The lower surface is the carbon cathode and the vertical surfaces are the walls of the cell and the sides of the anodes.

Table 3. Summary of the boundary conditions.

Boundary	Fluidic conditions	Electrical conditions
1	Pressure outlet	Isolated
2	User-defined function (UDF)	0 V
3	No slip wall	Imposed current density
4	No slip wall	Isolated

Table 3 shows that the boundary condition #2 (under the anodes) is the one that generates the gas using a user-defined function. In this function, the local current density is used to calculate gas generation at each location. From Table 3, we see that a 0 V condition has been imposed under the anodes, and that a current density is imposed at the cathode. A current density of 0.6 A/cm^2 was used for this simulation.

3.3 Modelling of the Anode Bottom Surface

The boundary condition of bubble production under the anodes was made similar to L. Kiss and S. Ponscak's model [4, 6, 7]. According to this model, the surface is divided into a large number of elementary cells, each containing a nucleation site, see Figure 4.

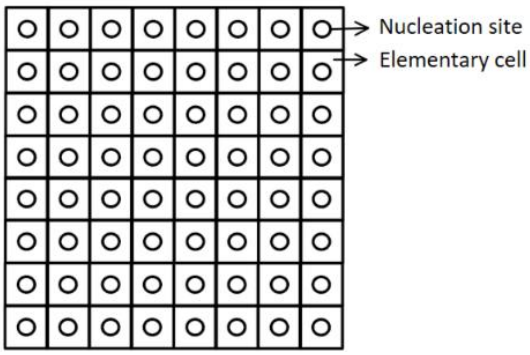

Figure 4. 2D anode surface division.

Since the model developed for this work is in 2D, rather than dividing a surface (rectangle) into squares, a line is divided into numerous 1 cm-long lines, according to Figure 5.

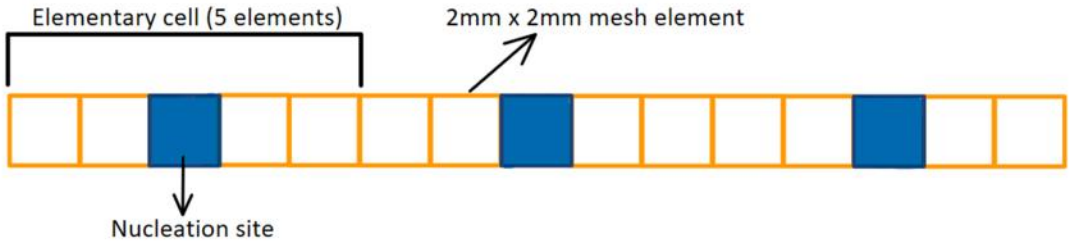

Figure 5. One dimension anode surface division.

The nucleation site corresponds to the mesh element at the center of an elementary cell (composed of five mesh elements of 2 mm). The UDF uses Faraday's law to calculate the mass of CO_2 generated by each elementary cell from the current flowing through its five mesh elements. The Faraday's law is given by:

$$m = \frac{i \cdot t \cdot M}{z \cdot F} \tag{3}$$

where:

m	Mass of aluminum produced, g
F	Faraday's constant (96 485.332 8959), C/mol
i	Electric current, A
t	Time, s
z	Number of electrons involved in the reaction
M	Molar mass, g/mol.

3.4 Fluid Properties

The properties of the fluids used have been influenced or based on the literature [5, 15, 18] and they are summarized in Table 4 and Table 5.

Table 4. Summary of the fluid's physical properties.

Fluid	Density [kg/m^3]	Viscosity [kg/(m·s)]	Electrical conductivity [S/m]
CO_2	0.4 [15]	$1.37 \cdot 10^{-5}$ [5]	$9 \cdot 10^{-6}$
Electrolyte	2050 [18]	0.003 [5]	220 [15]
Liquid aluminum	2500	0.0014	$3.5 \cdot 10^{6}$ [15]

Initial simulations demonstrated that the consequence of two-dimensional simulations generated BMI perturbations which were likely more important than industrial estimations. Rather than having several bubbles across the width of the anode, a single narrow, but very large bubble was present in the 2D models resulting in longer bubbles than it would be in 3D and resulting in greater disturbance to the BMI during evacuation of the bubbles. In order to proceed smoothly with the preliminary analysis performed with the 2D simulation and counterbalance this effect, it was necessary to overestimate the aluminum density to a value of 2500 kg/m^3 rather than 2270 - 2370 kg/m^3 [11, 15]. While this overestimation likely affects the overall magnitude of the phenomenon studied, all scenarios are affected similarly and the sensitivity analysis performed preserve its ability to pinpoint the factors with a dominant behavior.

Table 5. Summary of the surface tensions.

Fluid #1	Fluid #2	Surface tension [N/m]
CO_2	Electrolyte	0.132 [12]
Liquid Aluminum	CO_2	0.56 [11]
Liquid Aluminum	Electrolyte	0.8 [19]

4. Results

The aim of this work is to understand the effect of different input parameters on system responses. Thus, the input parameters studied in this work are the ACD, the width of the center channel and the presence or absence of chamfers at the corners of the anodes which are set at a 45° angle. On the other side, the output parameters studied are diverse: BMI deformation, turbulent kinetic energy, and the anode bubble coverage.

With these three input parameters, a Taguchi plan (Table 6) was used to limit the number of simulations required to four, since this work is a preliminary one and it intends to highlight the DOE opportunities for three-dimensional simulations.

Table 6. Design of experiments.

Case #	ACD [mm]	Center channel width [mm]	Presence of chamfer
1	40	80	No
2	40	200	Yes
3	60	80	Yes
4	60	200	No

In all these sections, results are analyzed between three and twenty seconds since the initial three seconds of the simulation are considered a stabilization period leading to steady state operations.

4.1 BMI Perturbation

In order to efficiently analyze the deformation of the BMI, a Python code was made to evaluate the maximum amplitude of the aluminum compared to its resting height at each instant. Deformation versus time for each case studied are presented in Figure 6 to 9.

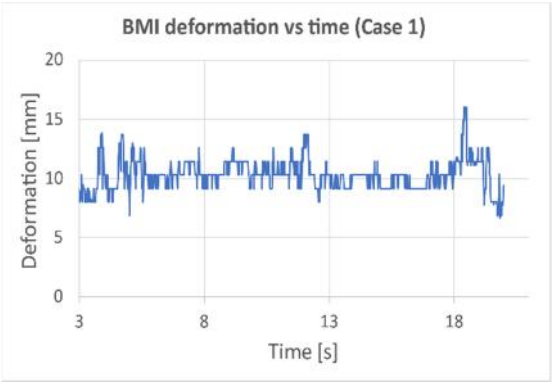

Figure 6. BMI deformation vs time (Case 1).

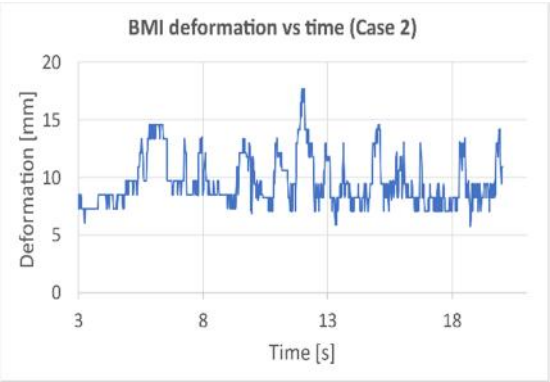

Figure 7. BMI deformation vs time (Case 2).

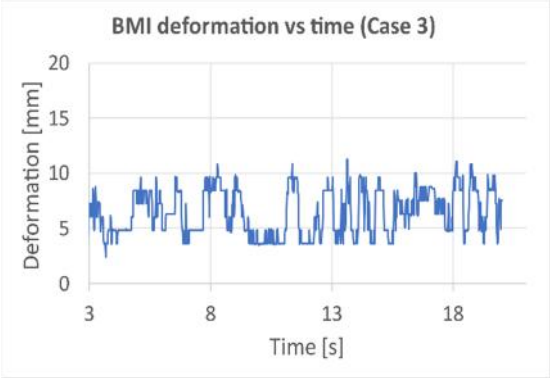

Figure 8. BMI deformation vs time (Case 3).

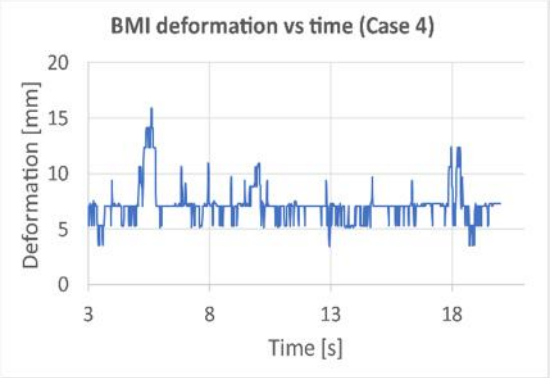

Figure 9. BMI deformation vs time (Case 4).

By averaging these deformations from three seconds to twenty seconds, an analysis was carried out to determine the effect of each parameter on the average BMI deformation.

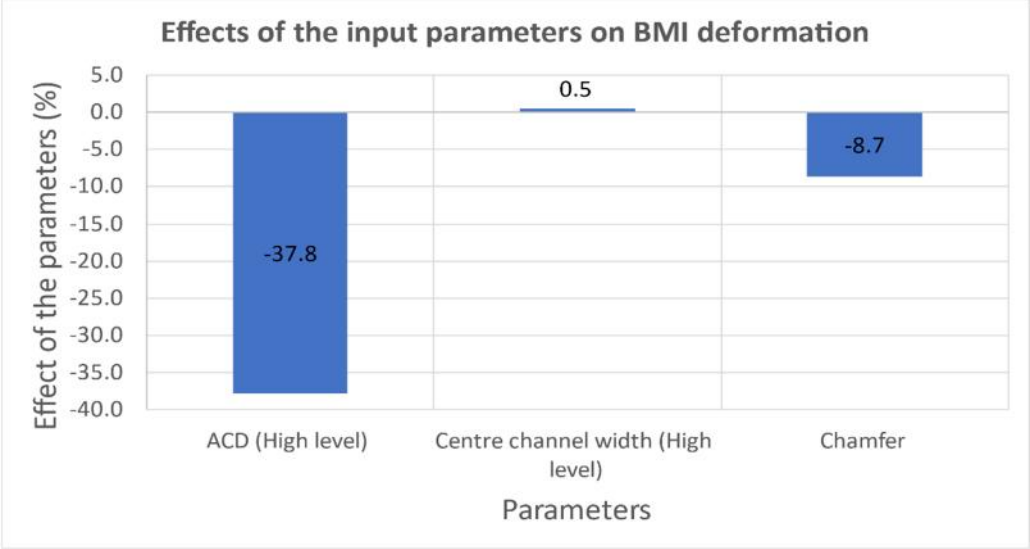

Figure 10. Effect of the input parameters on the mean BMI deformation.

Figure 10 shows that the parameter with the greatest influence is the ACD. Specifically, by looking at the higher ACD limits which corresponds to a 20 mm increase in ACD from the low ACD value, the results indicate a 37.8 % decrease in mean BMI deformation. Consequently, by reducing the ACD to smaller values, the BMI agitation would be increasing proportionally in a significant manner, leading to higher instability for the cell. Having tested this input parameters using only two levels, the observed behavior is considered linear. However, in the future thorough analysis, multiple levels will be required to confirm the exact behavior of this phenomenon, which is most likely non-linear.

Similarly, the presence of a chamfer reduces BMI deformation by around 8.7 %. Therefore, this feature may be of interest to limit the agitation of the metal pad in the initial days after an anode change. In the same line of thought, as the anode ages, its radius of curvature at the lower corners will increase due to the consumption of carbon resulting from electrolysis and oxidation. Assuming that this radius of curvature will have similar effect to that of a chamfer, as the anode ages, the BMI deformation tend to decrease leading to an increase in the cell stability after a certain threshold. Future studies will allow for a clearer investigation regarding the anode radius of curvature in order to better understand how long a new anode is affected by this instability and

to provide a comparison to study the potential business case that could lead for chamfer deployment.

Finally, the effect of the width of the central channel on BMI deformation is negligible as it is sufficiently wide to easily allow the evacuation of bubbles. In the event where this distance would become extremely small (equivalent to the width of a bubble's diameter), then it is possible that the effect may become significant. This consideration is non-probable due to geometrical challenges that would need to be assessed before reaching such small gaps.

4.2 Mixing in the Center and Side Channels

In order to better understand the effect of the input parameters on agitation in the central and side channels, the turbulent kinetic energies (TKE) were plotted. Figure 11 presents the effect of the input parameters on the TKE in the center and side channels.

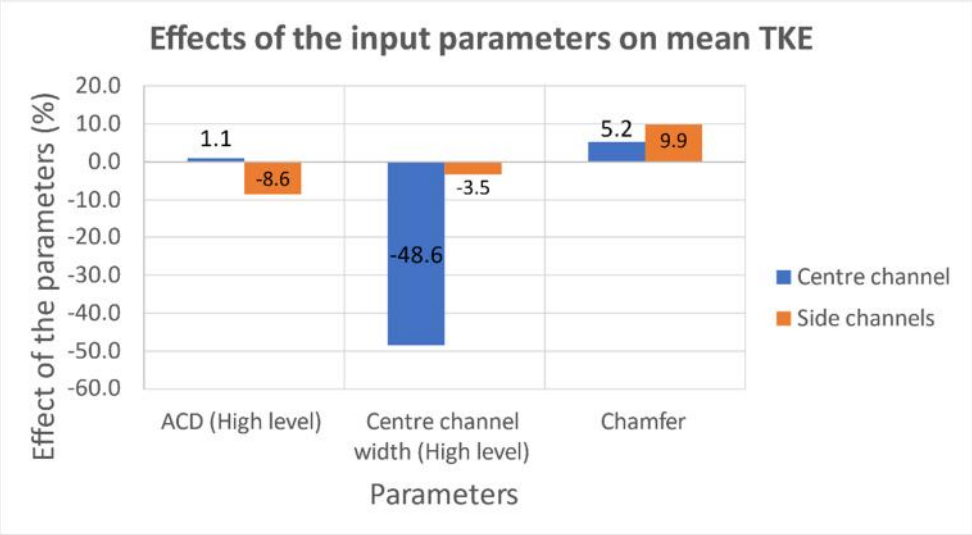

Figure 11. Effects of the input parameters on the mean TKE.

The effect of the distance between anodes in the center channel's TKE is very significant, giving a 48.6 % reduction for a 120 mm increase of the center channel width. This result is easy to understand, as the bubbles that escape are concentrated in a smaller volume. In contrast to the intuitive reasoning, the observed variation in TKE is not equivalent to the variation in width that was imposed. A reduction in TKE equal to the augmentation of distance between the anodes would be reasonable to expect, which would correspond to 150 % between the lower-level width (80 mm) and the high level (200 mm). However, we only find a 48.6 % reduction in TKE, which is three times less than the change in width. This is most probably due to the chaotic nature of the bubble behavior which generates a base level of turbulence in the flow independent of the volume of liquid displaced. Such line of investigation is extremely interesting to consider when an aluminum smelter is considering a temporary, or permanent change to the anode dimensions. While the liquid volume in between the anodes available to dissolve alumina will change, the mixing properties of this bath will be affected significantly as well. Thus, a simple geometry change may require adjustments in the feeding strategy to account for both these effects, the latter being often overlooked.

On another note, the presence of a chamfer increases the average TKE in the center channel by 5.2 % and in the side channels by 9.9 %. Although this effect is moderate, it can slightly improve alumina dissolution in the initial period following the anode change. However, the significant increase in the side channels may have the negative effect of affecting the side ledge behavior due

to increased turbulence. While the potential consequences on the ledge profile resulting from an increase in TKE are currently not estimated, future studies using the 3D model may provide insights that will help to prevent ledge degradation and to enhance cell life performances.

Finally, the ACD is the factor with the less notable impact. While it has no effect in the TKE in the center channel, it has a low effect in the side channels as an increase of 8.6 % in the TKE is observed when the ACD is reduced by 20 mm.

4.3 Anode Bubble Coverage

Anode covering and potential difference are closely linked, since gas bubbles have an insulating effect in the electrolytic cell. In this way, the anode bubble coverage was determined from the voltage, knowing the total current flowing through the anode and the resistance of the electrolyte. Figures 12 to 15 show the evolution of bubble coverage as a function of time for each studied case.

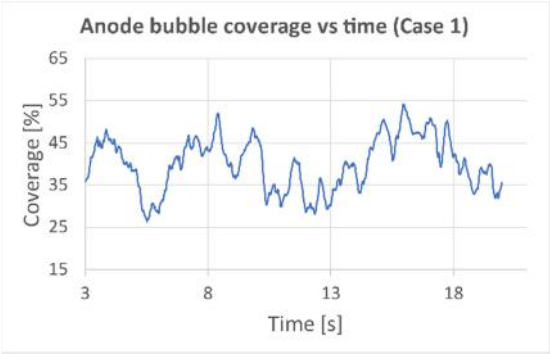

Figure 12. Anode bubble coverage vs time (Case 1).

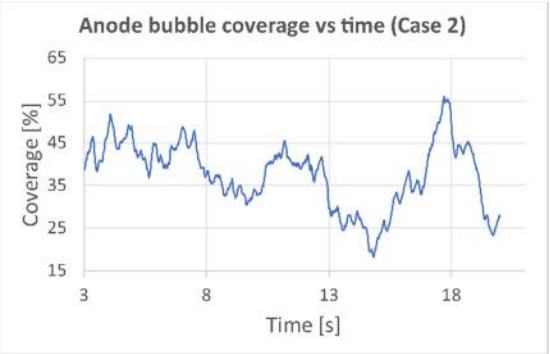

Figure 13. Anode bubble coverage vs time (Case 2).

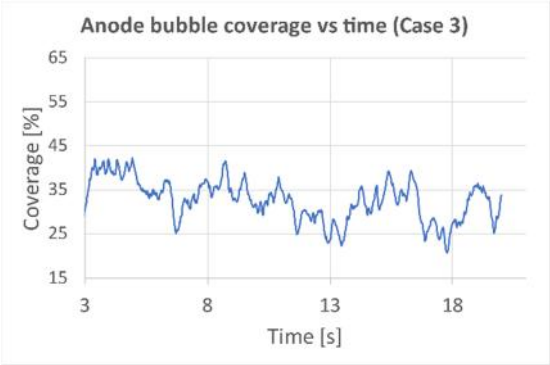

Figure 14. Anode bubble coverage vs time (Case 3).

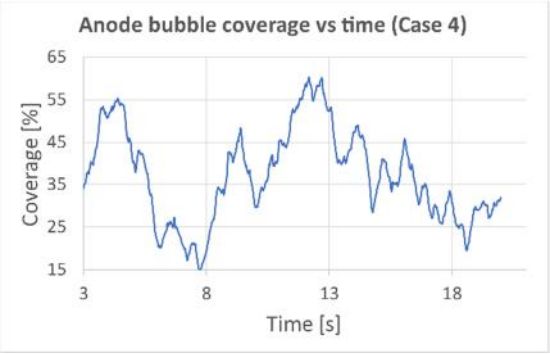

Figure 15. Anode bubble coverage vs time (Case 4).

These figures have been analyzed over the period 3-20 seconds and the effect of each factor is shown in figure 16.

Figure 16 shows that the presence of a chamfer considerably reduces bubble coverage (9.1 %). This effect occurs because the chamfer facilitates the escape of bubbles from under the anode, providing a smoother transition. A reduction in bubble coverage is desirable in most cases since the presence of gas increases resistance and hence the electrical power required. When investigating the same factors using the 3D model, it is very likely that the effect of the chamfer may become less significant as the anode slots will play the same role and thus reducing the impact of the anode extremities.

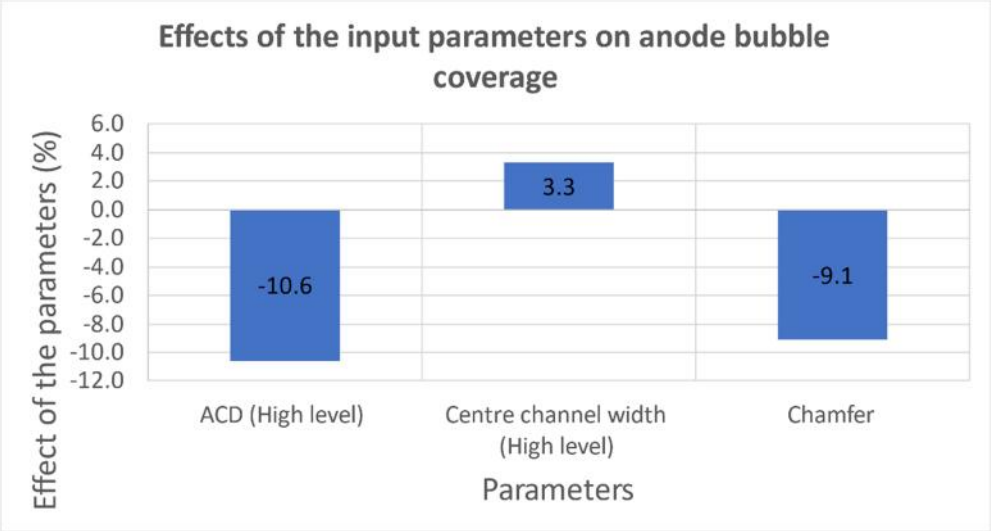

Figure 16. Effects of the input parameters on the mean anode bubble coverage.

Similarly, Figure 16 shows that increasing the ACD by 20 mm tends to reduce bubble coverage by around 10.6 %. This is the most surprising result. It was speculated that the anode bubble coverage would be inversely correlated with the BMI agitation, which would make it easier for the bubbles to be displaced, coalesce, and detach from underneath the anodes. If that hypothesis was correct, then a lower ACD should have reduced the bubble coverage. Since the opposite effect was observed, the initial hypothesis may be invalid, or there is another factor to take into consideration which has a bigger impact. For example, a plausible alternative hypothesis may be that the preferential bubble nucleation may differ due to different local density. In the case with higher ACD, the bubbles would then be generated more uniformly under the anode surface, while a narrower ACD would lead to a region with a more concentrated bubble generation. Such behavior could corroborate the results observed. Nonetheless, further study is required to clearly explain this behavior.

The effect of the distance between the anodes in the central channel is considered negligible, probably due to the same explanation as discussed for the absence of correlation with the BMI perturbation at the end of section 4.1.

5. Conclusions

The results obtained in this study are the first steps towards additional improvements to the understanding of bubble flow behavior. Namely, they highlighted the potential effects of different factors such as the distance between the anodes, the ACD, and the presence or absence of chamfer on output data such as turbulence in the lateral and central channels, the anode bubble coverage as well as the disturbance of the BMI.

Analysis of the results demonstrated the impact of ACD on BMI deformation. A 20 mm reduction in ACD causes an 37.8 % increase in mean agitation of the BMI. Also, the presence of chamfers reduces the deformation of the metal by providing a smoother escape for the bubbles.

Simulation results have also shown that the decrease in turbulence in the central channel is not equally proportional to the increase in channel width. In fact, the variation in TKE is about three times smaller. This analysis also showed that the presence of a chamfer increases the mean turbulence in the central and side channels by respectively 5.2 % and 9.9 %.

The last analysis in this study showed that chamfers reduce bubble coverage by an average of 9.1 %, but this effect remains to be verified under 3D simulations as it may be amplified by the absence of anode slots in the 2D simulations. Also, it was seen that a 20 mm increase in ACD had the effect of reducing anode bubble coverage by 10.6 %.

Since the generated model is 2D and not 3D, it is important to consider that the absolute values obtained when analyzing these results are unrepresentative in magnitude to the reality. Bubbles modeled in 2D have a much greater effect than bubbles modeled in 3D especially on BMI deformation, since they occupy the entire width of the anode. The mass of bath displaced by the evacuation of a 2D bubble is therefore more important than the mass displaced by a 3D bubble. Also, the absence of anode slots has a significant effect on the results. In the 2D model, the bubble escape locations are limited to the two corners, while in a real cell, a large portion of the bubbles escape through the slots. This effect will be important for each of the output parameters studied in this work. The deformation of the BMI, the turbulence in the central and lateral channels, as well as the bubble coverage of the anode, may be lower.

However, the likeliness that the dominant factors highlighted remain of interest as we move towards a 3D simulation is elevated. Thus, these results mainly serve to understand trends and to identify which variables are the most relevant to properly design and investigate the same effects using a three-dimensional model.

Therefore, the next step is to use the knowledge acquired in this study to create a 3D model of bubble flow beneath the anodes. By transitioning to a 3D model, the effects of anode slots, which are of great interest to the industry, will be considered in the analysis. Similarly, the numerical values obtained with the 3D model can be considered more reliable than those obtained in 2D.

6. References

1. Kai Grjotheim, Halvor Kvande, *Introduction to Aluminium Electrolysis: Understanding the Hall-Héroult Process,* Beuth Verlag GmbH, 1993, 268 pages.
2. Jomar Thonstad, *Aluminium Electrolysis: Fundamentals of the Hall-Héroult Process*, Aluminium-Verlag, 2001, 359 pages.
3. Pascal Lavoie, Mark P. Taylor and James. B. Metson, A review of alumina feeding and dissolution factors in aluminum reduction cells, *Metallurgical and Materials Transactions B*, Vol. 47, (2016), 2690-269.
4. Sándor Poncsák et al., *Formation et evolution des bulles de gaz au-dessous de l'anode dans une cuve d'electrolyse d'aluminium,* PhD Thesis, Université du Québec à Chicoutimi, Québec, Canada, 2000.
5. Kaiyu Zhang et al., Computational Fluid Dynamics (CFD) Modeling of Bubble Dynamics in the Aluminum Smelting Process, *Industrial & Engineering Chemistry Research*, Vol. 52, No. 33, (2013), 11378-11390.
6. László. I. Kiss and Sándor Poncsák, Effect of the bubble growth mechanism on the spectrum of voltage fluctuations in the reduction cell, *Light Metals* 2002, 217-224
7. László. I. Kiss, Sándor Poncsak, and Jacques Antille, Simulation of the bubble layer in aluminum electrolysis cells, *Light Metals 2005*, 559-564.
8. Morshed Alam et al., Investigation of Electrolytic Bubble Behaviour in Aluminum Smelting Cell, *Light Metals 2013*, 591-596.
9. Kaiyu Zhang et al., A numerical assessment of bubble-induced electric resistance in aluminium electrolytic cells, *Journal of Applied Electrochemistry*, Vol. 44, No. 10, (2014), 1081-1092.
10. Dagoberto S. Severo, et al., Modeling the Bubble Driven Flow in the Electrolyte as a Tool for Slotted Anode Design Improvement, *Essential Readings in Light Metals: Volume 2*

Aluminum Reduction Technology, G. Bearne, M. Dupuis, et G. Tarcy, Éds., Cham: Springer International Publishing, (2016), 409-414.

11. Kristian Etienne Einarsrud, et al., Towards a coupled multi-scale, multi-physics simulation framework for aluminium electrolysis, *Applied Mathematical Modelling*, Vol. 44, (2017), 3-24.
12. Kaiyu Zhang et al., Computational Fluid Dynamics (CFD) Modeling of Bubble Dynamics in the Aluminum Smelting Process, *Industrial & Engineering Chemistry Research*, Vol. 52, No. 33, (2013), 11378-11390.
13. Shuiqing Zhan et al., 3D Numerical Simulations of Gas–Liquid Two-Phase Flows in Aluminum Electrolysis Cells with the Coupled Model of Computational Fluid Dynamics–Population Balance Model" *Industrial & Engineering Chemistry Research*, Vol. 56, No. 30, (2017), 8649-8662, 2017.
14. Yuqing Feng et al., Two-Phase CFD Model of the Bubble-Driven Flow in the Molten Electrolyte Layer of a Hall–Héroult Aluminum Cell, *Metallurgical and Materials Transactions B*, Vol. 46, No. 4, (2015), 1959-1981.
15. A. Cubeddu, V. Nandana, and U. Janoske, A Numerical Study of Gas Production and Bubble Dynamics in a Hall-Héroult Reduction Cell, *Light Metals 2019*, 605-613.
16. ANSYS Fluent, *Version 15.0: User Manual,* ANSYS, Inc., Canonsburg, USA, 2013, 1080 pages.
17. Hongbo Liu, Liang-Ming Pan and Jian Wen, Numerical simulation of hydrogen bubble growth at an electrode surface, *The Canadian Journal of Chemical Engineering*, Vol. 94, No. 1, (2016), 192-199.
18. Nithin S. Panicker et al., Computational modeling and simulation of aluminium smelting process using OpenFOAM, *5th Thermal and Fluids Engineering Conference (TFEC),* 5-8 April 2021, Virtual conference.
19. B. J. Keene, Review of data for the surface tension of pure metals, *International Materials Reviews*, Vol. 38, No 4, (1993), 157-192.